Scanner-free and wide-field endoscopic imaging by using a single multimode optical fiber

Youngwoon Choi[1], Changhyeong Yoon[1], Moonseok Kim[1], Taeseok Daniel Yang[1], Christopher Fang-Yen[2], Ramachandra R. Dasari[3], Kyoung Jin Lee[1], and Wonshik Choi[1,*]

[1]*Department of Physics, Korea University, Seoul 136-701, Korea*

[2]*Department of Bioengineering, University of Pennsylvania, Philadelphia, Pennsylvania 19104, USA*

[3]*G. R. Harrison Spectroscopy Laboratory, Massachusetts Institute of Technology, Cambridge Massachusetts 02139, USA*

Methods

Detailed description of LMSF experimental setup

The schematic diagram of the experimental setup is shown in Fig. 1 of the main text. Here we introduce detailed experimental setup of LMSF in Fig. S1(a). A He-Ne laser beam with a wavelength of 633 nm is split by BS1. One is reflected off at the 2-axis galvanometer mirror (GM: Cambridge Technology) and delivered to the input plane (IP) of the fiber via a polarizing beam splitter (PBS) and an objective lens (OL: 40X, ACHN40XP, Olympus). This beam propagates through the optical fiber and illuminates an object (USAF target: NT55-622, Edmund Optics Inc.) located at the object plane (OP). The reflected beam by the object propagates back through the fiber to the IP. The beam is then collected by the same objective lens and relayed to the camera. The other beam divided at the BS1 propagates through free space and is combined with the reflected wave from the object at BS3, making interference at the camera. Instead of BS2

schematically shown in Fig. 1, we employed a half wave plate (HWP) and a PBS in the experiment for enhancing the contrast of interference.

A brief schematic diagram is shown in Fig. 2(b) of the main text for the measurement of a transmission matrix. In the experiment, we installed additional optical components on top of the existing LMSF setup. As shown in Fig. S1(b), the laser beam steered by the GM is guided directly to the OP via a lens and an additional objective lens (OL_T, 20X, ACHN20XP, Olympus) whose focal plane matches the OP of the fiber. Then, the beam couples to the fiber at OP and propagates through the fiber toward the IP. The transmitted wave is collected by the OL and the interference image is captured by the camera. By steering the GM we scan the illumination angle $(\theta_\xi, \theta_\eta)_T$ at OP and record transmitted waves at various incident angles.

Measured transmission matrix

Some of representative amplitude images of the measured transmission matrix elements are shown in Fig. 2(a) in the main text. Here we present some of the amplitude images (Fig. S2(a)) and their corresponding phase images (Fig. S2(b)) in Fig. S2. The phase maps of the transmission matrix element are randomly distributed in the range of $-\pi$ to π. And the mean size of the random speckle becomes finer as the input angle $(\theta_\xi, \theta_\eta)_T$ is increased since the coupling into the higher order mode is significant.

Turbid Lens Imaging (TLI) Algorithm

The equation (1) in the main text explains how to reconstruct an object image at the OP, $E_{OP}(\xi, \eta)$, from the distorted image, $E_{IP}(x, y)$, recorded at IP. Although a similar method of image reconstruction is well explained in our previous report for the study of a disordered medium[1,2], the Eq. (1) is more accurate in that the relation is legitimate even when the set of angular plane

waves form an overcomplete basis. The detailed derivation of Eq. (1) is introduced in the following.

In the Fig. 2(b) in the main text, the image at the OP is delivered to the IP through the fiber in a complicated way. But it is possible to deduce the original image at the OP from the image at IP if we have the knowledge on the input-output response of the fiber from OP to IP. The figure 2(a) in the main text shows this knowledge as the form of output images at IP for various angular plane wave inputs at OP. But the use of this information is not straightforward in itself because the measured data describes the relation between the angles of waves at OP, not the position, and the positions at IP.

To make the reconstruction process straightforward, we construct a transmission matrix T (x, y; ξ, η) that describes complex field at (x, y) in the IP for the optical waves incident at a point (ξ, η) in the OP. Let us first define a set of complex field images in Fig. 2(a) as E_{fiber} (x, y; θ_ξ, θ_η), which means a complex field amplitude at (x, y) in the IP for a certain incident angle (θ_ξ, θ_η) at the OP. The subscript *fiber* indicates that the complex field map is measured for the transmitted waves through the fiber. In order to construct a transmission matrix, T, we need to know the complex field map, E (ξ, η; θ_ξ, θ_η), for the incident angle (θ_ξ, θ_η). This is done simply, as a one-time calibration procedure, by measuring the complex field at the OP while changing the incident angle.

With E_{fiber} (x, y; θ_ξ, θ_η) and E (ξ, η; θ_ξ, θ_η) at hand, we can construct T (x, y; ξ, η) in the following procedure. We first obtain E (θ_ξ, θ_η; ξ, η) which is the complex field at (θ_ξ, θ_η) for an incident wave at (ξ, η), by inverting the matrix E (ξ, η; θ_ξ, θ_η). Based on the completeness of the angular plane wave basis, the transmission matrix can be obtained by the following relation:

$$T(x,y;\xi,\eta)=\sum_{\theta_\xi,\theta_\eta}E_{fiber}(x,y;\theta_\xi,\theta_\eta)E(\theta_\xi,\theta_\eta;\xi,\eta). \quad (2)$$

Once this transmission matrix is constructed, the relation between $E_{OP}(\xi, \eta)$ and $E_{IP}(x, y)$ can be described in a straightforward manner as follows:

$$E_{IP}(x,y) = \sum_{\xi,\eta} T(x,y;\xi,\eta) E_{OP}(\xi,\eta). \quad (3)$$

Then, the $E_{OP}(\xi, \eta)$ can be obtained by applying the inversion of T for the $E_{IP}(x, y)$, which is the Eq. (1) in the main text.

The Effect of Fiber Bending on the Image Reconstruction

As shown in the Fig. 3 of the main text, LMSF is working well under the scanning operation of the fiber end. Moving one end of the fiber away from the initial position causes the change in the shape of the fiber. This modifies the transmission matrix since the wave propagation through the multi-mode fiber is very susceptible to the shape of the fiber. However, we found that most of the transmission matrix elements remain nearly intact with the modification of the fiber shape to a certain extent. Especially, those matrix elements whose input angle is large remain almost the same upon the bending of the fiber.

We characterize the effect of fiber bending on the transmission matrix by comparing transmission matrices measured at different radii of curvature of the fiber. As illustrated in Fig. S3(a), several transmission matrices are measured up to the incident angular coverage of 0.41 NA while varying the fiber shape. Specifically about 30 cm-long middle part of the fiber is taken and the center position is translated up to ± 5 mm from the initial position. The cross-correlation between the initial transmission matrix and that at the translated position is calculated to quantitatively assess the similarity of them. The figure S3(b) shows the map of correlation with respect to the incident angle for various translations. One can notice that the matrix elements stay correlated to the wide range of distortion. This robustness of modes to the bending has led to the successful image reconstruction in the LMSF under endoscopic surveying operation.

Finally, we test the working range of the scanning view field in LMSF. The fiber end and the USAF target are mounted on the same translation stage, and the stage is moved along the OP plane. In this way, identical part of the target is imaged while the fiber end is scanned. The range of translation is set from -5 mm to +5 mm with respect to the original position. As shown in Fig. S3(c), the target image is well resolved for the entire scanning range. This demonstrates that the view field can be scanned by at least 10 mm-long travel of the fiber end with the reasonable imaging quality.

Numerical refocusing for 3D imaging

Since we obtain the complex field images (Fig. 2(c) in the main text) at the input plane, we can acquire complex field images of the target object at the OP (Fig. 2(d)). Then, we numerically propagate each of those images taken at the OP and construct an image at a different plane located away from OP. The complex field image at the OP, $E_{\mathrm{OP}}(\xi, \eta; z=0)$, can be decomposed into a superposition of many plane wave components by the inverse Fourier transformation:

$$E_{OP}(\xi,\eta;z=0)=\iint F(k_\xi,k_\eta)\exp\left[-i(k_\xi\xi+k_\eta\eta)\right]dk_\xi dk_\eta. \quad (4)$$

Here $z = 0$ stands for the OP, $F(k_\xi, k_\eta)$ the Fourier transform of $E_{\mathrm{OP}}(\xi, \eta; z = 0)$, and (k_ξ, k_η) the wave vector conjugate to the (ξ, η). In order to propagate the images along z-axis by the distance d, the free space transfer function $H(k_\xi,k_\eta)=\exp(-id\sqrt{k_0^2-k_\xi^2-k_\eta^2})$ is multiplied on the $F(k_\xi, k_\eta)$. Here $k_0 = \lambda/2\pi$ is the wavenumber in the free space. The propagated image is then constructed by the following inverse Fourier transformation:

$$E_{OP}(\xi,\eta;z=d)=\iint H(k_\xi,k_\eta)F(k_\xi,k_\eta)\exp\left[-i(k_\xi\xi+k_\eta\eta)\right]dk_\xi dk_\eta. \quad (5)$$

After performing the numerical propagation for all the individual images in Fig. 4(b), we obtain the refocused LMSF image at the desired focus.

Materials

Instruments and software

A He-Ne Laser (25-LHP-928-230, Melles Griot) is used for the illumination source. A 1 meter long multimode optical fiber (BFL48-200, Thorlabs) with 200 μm core diameter and 0.48 NA is used for a flexible LMSF. A high-speed CMOS camera (M3, RedLake, 500 fps) is used for recording interference images and a two-axis galvanometer scanner (Cambridge Technology) is used for steering the illumination beams at the facet of the fiber. A USAF target (NT55-622, Edmund Optics Inc.) is used as a non-biological sample and villi structures extracted from intestines of a rat is used as a biological specimen**.** The MATLAB™ software is used for constructing transmission matrix and further image processing. Specifically, the built-in function, *pinv*, is used for obtaining the pseudo-inverse of the measured transmission matrix which is not a square matrix in general.

Tissue preparation

The villi tissue used as a specimen in Fig. 3 was prepared from the gut of Sprague Dawley rat (Charles River, OrientBio Inc.) of 1-2 postnatal days. After administrating anesthesia with zoletil 50, the 1 cm-long intestine organ is extracted. A slice of the tissue is placed on a coverglass and the uncovered side of the tissue is faced at the fiber. All the experimental procedures and protocols were in accordance with the guidelines established by the Committee of Animal Research Policy of Korea University College of Medicine.

Supplemental Movie

Movie 1. Image reconstruction process in LMSF. Image reconstruction process explained in Figure 2 in the main text is displayed in detail. The angles shown on the left are the illumination angle, $(\theta_x, \theta_y)_S$, and the figure on the left is the corresponding distorted object image

measured by the camera. The figure in the middle presents the reconstructed image after applying TLI algorithm to the image on the left. The figure on the right is the accumulated average of the figure in the middle for the implementation of speckle imaging, which results in the clean object image.

Supplemental Figures

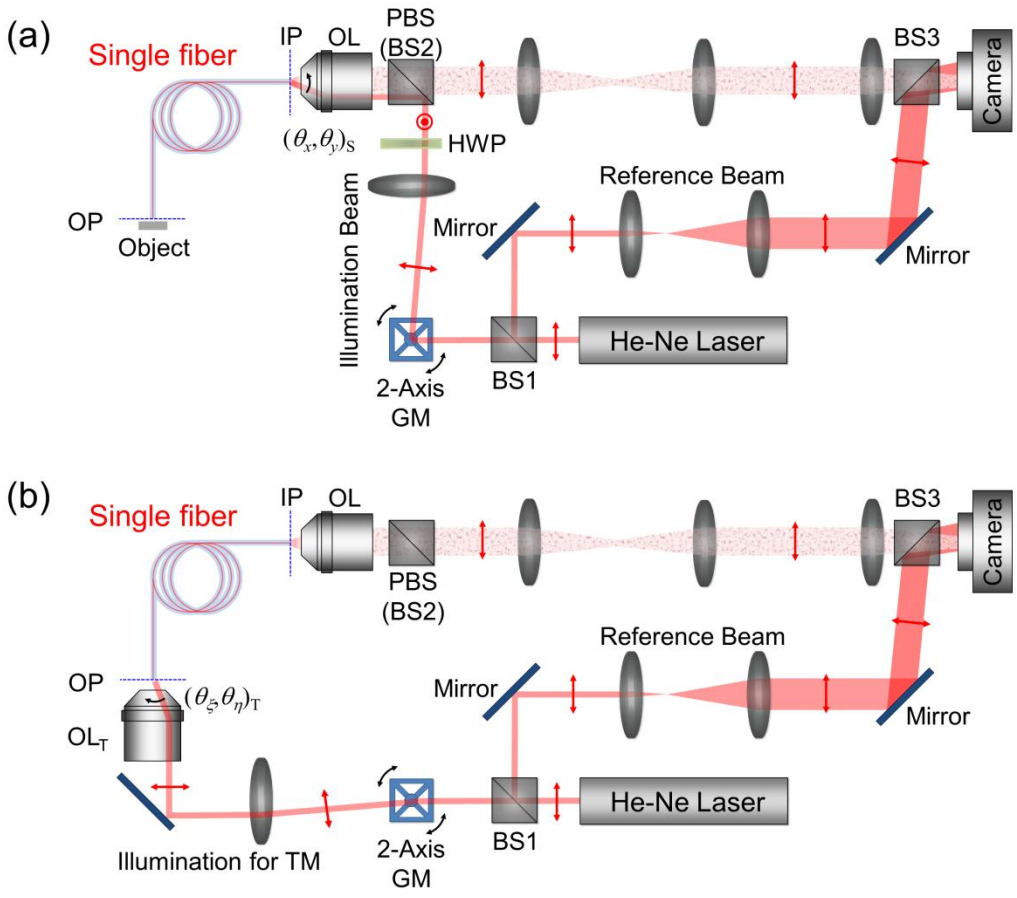

Figure S1. Detailed experimental setup. (a) A detailed setup for LMSF. A half wave plate and a polarizing beam splitter are used instead of BS2 mentioned in the main text. (b) A setup for the measurement of transmission matrix. OL_T: objective lens, PBS: polarizing beam splitter, BS1 and BS3: beam splitters, GM: galvanometer mirror, OP: object plane, IP: input plane.

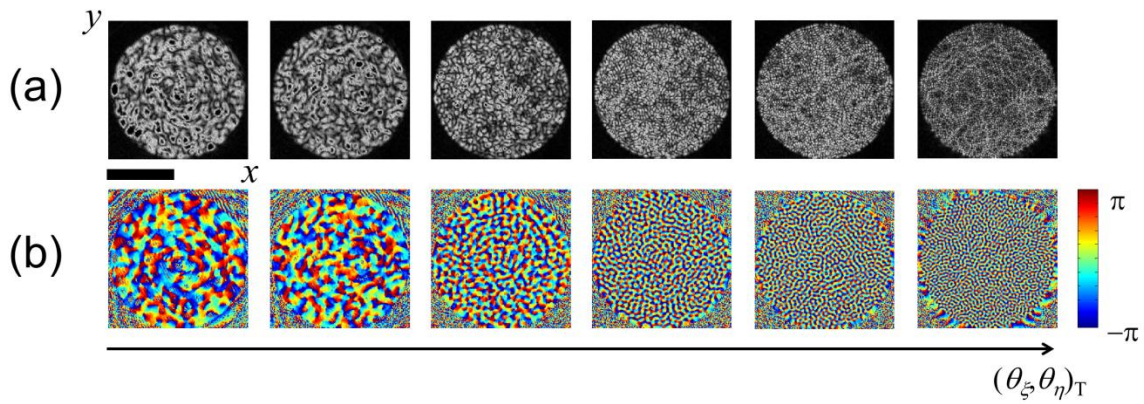

Figure S2. Measured transmission matrix elements. (a) Amplitude and (b) phase of the measured transmission matrix elements of the single multi-mode optical fiber. The wavefront of the plane wave input is distorted after passing through the fiber as a function of incident angle. Scale bar: 100 μm.

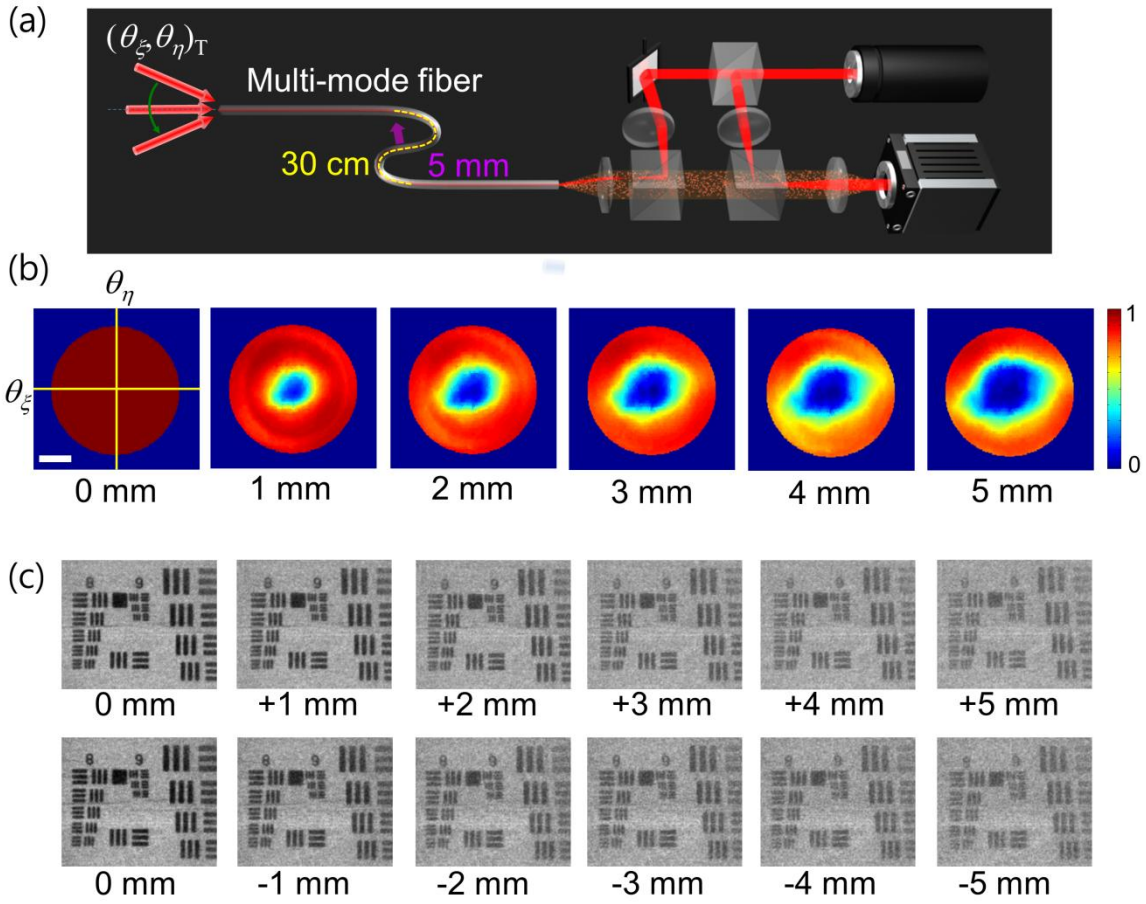

Figure S3. The effect of bending on the image reconstruction. (a) Measurement of transmission matrices while varying the fiber shape. The center point in the 30 cm-long middle part of the fiber is translated to control the degree of fiber bending. (b) Maps of cross correlation between the transmission matrix at the initial position (left) and those at the translated position with respect to the incident angle. Scale bar: 0.2 NA. Color bar, normalized cross correlation. (c) LMSF images under endoscopic surveying operation of the fiber end. The numbers below the figures indicate the displacement of the fiber end with respect to the original position.

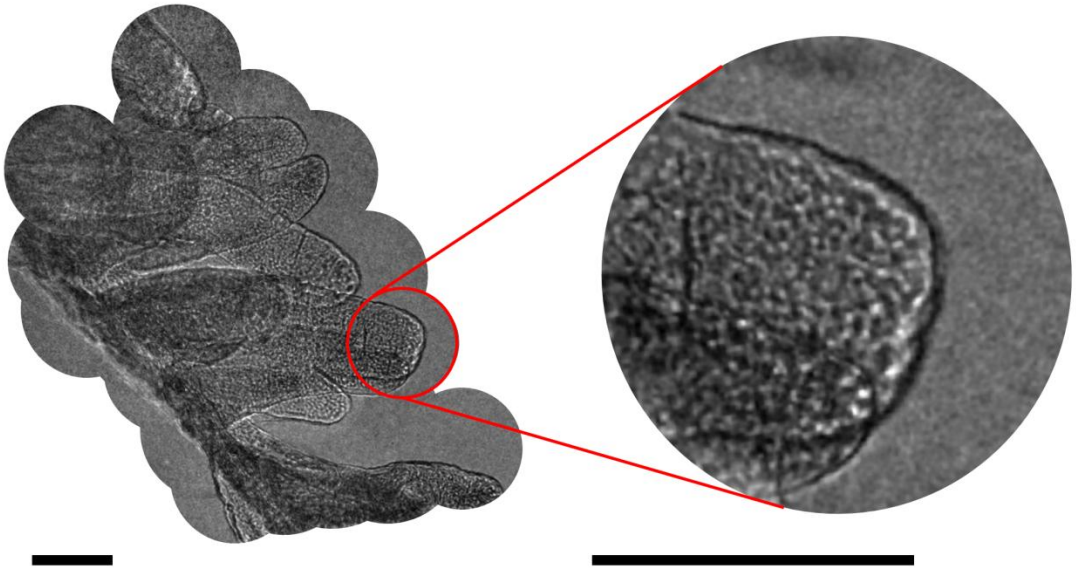

Figure S4. Zoom-in view of the villi. The image on the left is the same as that in Fig. 4(b) of the main text. The villi in the red circle is magnified and shown on the right-hand side for the clear visibility. Scale bars: 100 μm.

1 Choi, Y. *et al.* Overcoming the Diffraction Limit Using Multiple Light Scattering in a Highly Disordered Medium. *Phys Rev Lett* 107, 023902 (2011).

2 Choi, Y. *et al.* Synthetic aperture microscopy for high resolution imaging through a turbid medium. *Opt Lett* 36, 4263-4265 (2011).